

Zero-shot Multi-Contrast Brain MRI Registration by Intensity Randomizing T1-weighted MRI (LUMIR25)

Hengjie Liu^{1,2}, Yimeng Dou³, Di Xu¹, Xinyi Fu¹, Dan Ruan² and Ke Sheng¹

¹ University of California, San Francisco, San Francisco CA, USA

² University of California, Los Angeles, Los Angeles CA, USA

³ University of Wisconsin, Madison WI, USA

Abstract. In this paper, we summarize the methods and results of our submission to the LUMIR25 challenge in Learn2Reg 2025, which achieved 1st place overall on the test set. Extended from LUMIR24, this year’s task focuses on zero-shot registration under domain shifts (high-field MRI, pathological brains, and various MRI contrasts), while the training data comprises only in-domain T1-weighted brain MRI. We start with a meticulous analysis of LUMIR24 winners to identify the main contributors to good monomodal registration performance. To achieve good generalization with diverse contrasts from a model trained with T1-weighted MRI only, we employ three simple but effective strategies: (i) a multimodal loss based on the modality-independent neighborhood descriptor (MIND), (ii) intensity randomization for appearance augmentation, and (iii) lightweight instance-specific optimization (ISO) on feature encoders at inference time. On the validation set, our approach achieves reasonable T1-T2 registration accuracy while maintaining good deformation regularity.

Keywords: Deformable Image Registration, Multimodal Registration, Deep Learning, Domain Shift, Foundation Model, MIND

1 Introduction

The LUMIR24 challenge introduced a large-scale dataset for monomodal T1-weighted brain MRI registration [1,2] and yielded fruitful results demonstrating the strength of deep learning in deformable image registration [3]. The winning method, SITReg [4], succeeded by emphasizing registration-specific inductive biases, including multi-resolution pyramid, by-construction inverse consistency (IC), group consistency (GC) and topological preservation, without resorting to complicated network architectures or advanced computation blocks such as Transformers or Mamba. The best-performing baseline, vector field attention (VFA) [5], was also notable for using a deterministic module to extract displacement directly from correlation features. Their success resonates with the recent studies that argue registration-specific designs matter more than choices of computation blocks [6–9]. Building on these insights, we closely examined the LUMIR24 leaders to identify the key “recipe” for strong monomodal registration.

As LUMIR25 shifts toward a foundation model capable of zero-shot registration while being trained only on T1-weighted images, we adopt three simple yet effective

strategies to handle multimodal settings: (i) a multimodal loss based on the modality-independent neighborhood descriptor (MIND) [10]; (ii) intensity augmentation using smooth randomized mappings, and (iii) lightweight instance-specific optimization (ISO) applied only to the feature encoders (excluding deformation prediction modules).

2 Methods

2.1 Key components for monomodal registration (LUMIR24)

We start by investigating key registration-specific designs that are critical to registration performance inspired by [4–7]. This includes the multiresolution pyramid, correlation calculation, and inverse consistency. We design a unified framework to test the contribution of each component, as detailed in Figure 1 and Table 1. More details can be found in [8].

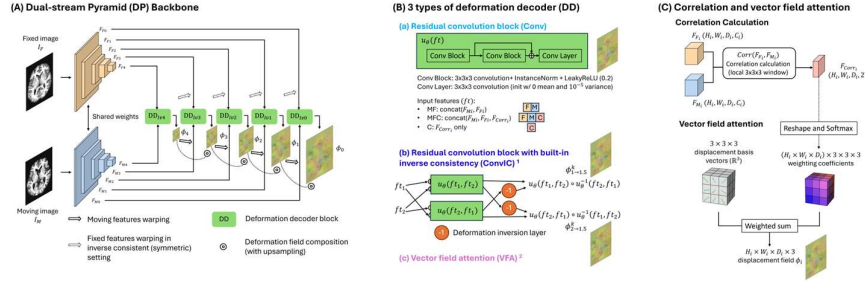


Fig. 1. (A) The standardized dual-stream pyramid (DP) backbone for registration. (B) Three types of deformation decoders. (C) Illustration of correlation calculation and vector field attention.

Table 1. High level summary of proposed methods and comparing methods.

Methods	Coarse-to-fine	Inverse consistency	Input features	Params (M) (encoder/decoder)
VoxelMorph	✗	✗	F M	0.3
TransMorph	✗	✗	F M	46.56
VFA	✓	✗	C	2.01
SITReg	✓	✓	F M	15.08
(a) DP-Conv-MF	✓	✗	F M	(0.51/2.35) 2.85
(a) DP-Conv-MFC	✓	✗	F M C	(0.51/2.66) 3.17
(a) DP-Conv-C	✓	✗	C	(0.51/1.49) 1.99
(b) DP-ConvIC-MF	✓	✓	F M	(0.51/2.35) 2.85
(b) DP-ConvIC-C	✓	✓	C	(0.51/1.80) 2.31
(c) DP-VFA	✓	✗	C	(0.51/0.28) 0.79

The registration results on LUMIR24 validation set are shown in Table 2. The multi-resolution pyramid is key to achieving better accuracy compared with VoxelMorph [11] and TransMorph [12] baselines. The inverse-consistent (IC) variants further improve regularity, as indicated by a lower non-diffeomorphic volume (NDV) [13]. Further, the correlation-only variants with less parameters surpass their counterparts, highlighting the role of correlation in deformation estimation.

However, in practice, correlation layers are very memory intensive. Under our GPU limits (48G of VRAM), scaling a larger backbone without correlation outperformed a smaller, correlation-based model. In addition, the group consistency (GC) loss and the NDV loss—introduced by last year’s winner—were highly effective at reducing HD95 and NDV, respectively. Consequently, we still base our final model on SITReg’s inverse-consistent framework, and include GC and NDV losses.

Table 2. Results on LUMIR 24 validation set. Results with * were obtained from the challenge reported validation leaderboard.

Methods	Dice \uparrow	HD95 \downarrow	TRE \downarrow	NDV (%) \downarrow
*VoxelMorph	0.7186 ± 0.0340	3.9821	3.1545	1.1836
*TransMorph	0.7594 ± 0.0319	3.5074	2.4225	0.3509
(a) DP-Conv-MF	0.7713 ± 0.0290	3.3534	2.4676	0.4158
(a) DP-Conv-MFC	0.7730 ± 0.0291	3.3566	2.4449	0.4672
(a) DP-Conv-C	0.7747 ± 0.0295	3.3666	2.4135	0.3795
(b) DP-ConvIC-MF	0.7717 ± 0.0288	3.3489	2.3660	0.0310
(b) DP-ConvIC-C	0.7724 ± 0.0288	3.3873	2.3357	0.0309
(c) DP-VFA	0.7764 ± 0.0284	3.2157	2.4420	0.0540
*VFA	0.7726 ± 0.0286	3.2127	2.4949	0.0788
*SITReg	0.7742 ± 0.0291	3.3039	2.3112	0.0231
*SITReg (GC/NDV)	0.7805 ± 0.0287	3.1187	2.3005	0.0025

2.2 Extension to multimodal registration (LUMIR25)

MIND loss. Our first adaptation for multimodal registration is to use a MIND-based similarity loss [10] instead of normalized cross correlation (NCC). The loss function is

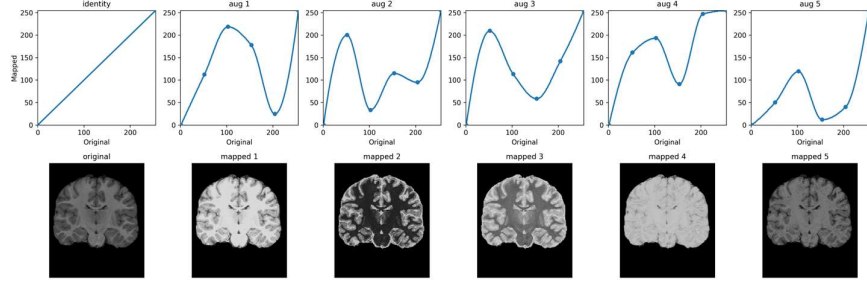
$$Loss = \lambda_1 L_{sim} + \lambda_2 L_{smooth} + \lambda_3 L_{GC} + \lambda_4 L_{NDV}, \quad (1)$$

where $\lambda_1 = 1$ for NCC and $\lambda_1 = 10$ for MIND, $\lambda_2 = 1$ with a diffusion regularizer, and $\lambda_3 = 40$ and $\lambda_4 = 1e-5$ as in SITReg. Although all LUMIR24 participants used NCC loss [3], we find that MIND performs competitively with NCC on LUMIR24 (Table 3). Notably, it improves TRE, which is expected since MIND is sensitive to edge and corner structures. Adding GC and NDV losses further improves accuracy for MIND as well.

Table 3. Comparison of NCC loss vs MIND loss on LUMIR24 validation set.

Methods	Dice \uparrow	HD95 \downarrow	TRE \downarrow	NDV (%) \downarrow
SITReg-NCC	0.7735 ± 0.0285	3.3183	2.3266	0.0267
SITReg-NCC (GC/NDV)	0.7798 ± 0.0289	3.1296	2.3102	0.0024
SITReg-MIND	0.7705 ± 0.0276	3.3781	2.2702	0.1045
SITReg-MIND (GC/NDV)	0.7761 ± 0.0290	3.0685	2.3139	0.0067

Intensity augmentation. Intensity augmentation has been widely used in domain generalization for medical image segmentation [14]. To mimic inter-sequence appearance shifts while preserving anatomy, we apply a smooth, randomized pointwise intensity remapping to each T1-weighted training volume. Specifically, we construct a 256-level lookup table $g: \{0, \dots, 255\} \rightarrow \{0, \dots, 255\}$ by randomly sampling $n_{knots} = 6$ control points, while enforcing $g(0) = 0$, $y_1 = 0$, and $y_{n_{knots}} = 255$ (4 control points are changing). A shape-preserving piecewise-cubic Hermite interpolant (PCHIP) yields a C^1 mapping without overshoot; the remapped image is obtained via $v' = g(v)$ for all voxels v . To avoid degenerate contrast collapse, we reject candidates whose post-mapping histograms show saturated bins using a preset threshold. Examples of augmented images are shown in Figure 2. In total, we generated 2,000 mappings for training.

**Fig. 2.** Intensity randomization examples for multimodal emulation. Aug #4 will be rejected.

ISO strategy. In LUMIR24, SITReg outperformed other methods without relying on ISO; however, ISO has been reported to enhance robustness for zero-shot tasks [3]. ISO is more relevant for multimodal registration: although our augmentation is diverse, it cannot fully reproduce real-world MRI contrasts. So, we chose not to use ISO for T1-T1 tasks and experimented with ISO for other modalities. While ISO decreases the overall loss, it can overfit to intensity matching. Empirically, we observed reduced HD95 with strong GC regularization, but pairwise ISO may break this regularization and slightly worsen HD95. To mitigate this, we apply ISO only to the feature encoder (ISO-fe), keeping the deformation decoders fixed. This is reasonable because the decoder has already seen diverse feature styles from augmentation, whereas adapting the encoder helps accommodate unseen intensity profiles with limited risk of overfitting. Also, ISO-fe only updates 22% of the total parameters compared to ISO-full. We ran both ISO-fe and ISO-full for 20 steps with the same loss function in Eq. 1 while

omitting the GC term. As summarized in Table 4, both ISO variants improve Dice but worsen HD95; ISO-fe yields better Dice and HD95 than ISO-full.

Table 4. Effect of ISO on multimodal registration (9 pairs)

Methods	Dice \uparrow	HD95 \downarrow	NDV (%) \downarrow
SITReg-MIND-Aug	0.7165 ± 0.0238	2.7409 ± 0.1777	0.0044 ± 0.0008
SITReg-MIND-Aug + ISO-full	0.7236 ± 0.0276	2.8723 ± 0.1907	0.0049 ± 0.0007
SITReg-MIND-Aug + ISO-fe	0.7241 ± 0.0284	2.8328 ± 0.1977	0.0048 ± 0.0007

2.3 Submitted method

Our final submission integrates two models. For T1-T1 registration, we use SITReg-NCC (GC/NDV) without ISO, as it performs slightly better than SITReg-MIND (GC/NDV). For all other imaging contrast pairs, we use SITReg-MIND-Aug (GC/NDV), with ISO-fe applied at inference time.

The models were implemented in PyTorch 2.5.1, and all training was conducted on NVIDIA RTX 6000 Ada GPUs with 48 GB of memory. Group consistency training required three GPUs to process three image pairs in parallel, whereas ISO could be performed on a single GPU.

3 Results

The validation set comprises 36 registration pairs in total: 18 in-domain (ID) T1-T1 pairs (9 evaluated with contours and 9 with landmarks), 9 out-of-domain (OD) high-field T1-T1 pairs evaluated with contours, and 9 multimodal (MM) T1-T2 pairs evaluated with contours. Our final validation results are shown in Tables 5 and 6. For reference we also list the synthSR baselines which convert T2 to T1 images using image synthesis [15] and then apply a monomodal registration model (SITReg or VFA).

Table 5. Registration results on the LUMIR25 validation set.

Methods	Dice \uparrow	HD95 \downarrow	TRE \downarrow	NDV (%) \downarrow
Final submission	0.7570 ± 0.0322	3.0388 ± 0.2989	2.3099 ± 0.2704	0.0030 ± 0.0012
SITReg + synthSR	0.7610 ± 0.0281	2.9968 ± 0.3322	2.3102 ± 0.2707	0.0024 ± 0.0004
VFA + synthSR	0.7536 ± 0.0260	3.1075 ± 0.3320	2.4956 ± 0.3783	0.0074 ± 0.0050

Table 6. Registration results on the LUMIR25 validation set (cont.).

Methods	Dice(ID)	Dice(OD)	Dice(MM)	HD95(ID)	HD95(OD)	HD95(MM)
Final submission	0.7816	0.7652	0.7240	3.1095	3.1740	2.8329
SITReg + synthSR	0.7816	0.7652	0.7363	3.1096	3.1743	2.7065
VFA + synthSR	0.7744	0.7545	0.7320	3.2033	3.2963	2.8228

4 Discussion

The proposed method—SITReg backbone with GC/NDV regularization, MIND-based similarity, intensity randomization, and encoder-only ISO—can perform multimodal registration despite being trained only on T1-weighted images. Overall, the recipe is simple, effective and robust. On the validation set, the proposed method is slightly inferior to synthSR-based baselines on T1-T2 registration metrics. Still, it may be more robust when synthesis fails or hallucinates contrast, because our pipeline does not assume a fixed intensity model.

However, there remains a clear accuracy gap across in-domain, out-of-domain, and multimodal validation, indicating room for improvement. A better-designed augmentation scheme that includes local varying effects and more realistic contrast mimicking may narrow this gap without introducing additional complexity of synthesis. Adding a correlation layer could further help multimodal matching, but we must first address memory limits to realize its benefit at useful scales.

The final test results confirm that our submitted solution works well for all T1-T1 registration tasks (both in-domain and out-of-domain), but falls short on multimodal tasks. The strong performance on T1-T1 tasks is attributed to the successful strategies in SITReg. Using MIND loss as we experimented or MIND features as in [16] can improve robustness to out-of-domain contrast variations, but may slightly reduce contour-matching metrics in this particular challenge. Nevertheless, these strategies may still be helpful for more diverse clinical data. MIND loss is also beneficial for improving landmark matching (TRE) due to its structure-driven nature.

Finally, we want to highlight **the importance of registration-specific inductive biases**, including multi-resolution pyramids, inverse consistency, group consistency, topological preservation/diffeomorphism, and correlation-assisted correspondence establishment. *These ideas are not new, yet they are often overlooked or underexplored in many (if not most) trend-driven learning-based methods.* We also found the correlation-only models very promising. The idea was proposed early in deep learning-based optical flow research [17]. Correlation-only models can achieve superior results compared to intensity-feature-only and intensity+correlation variants, while using fewer parameters. Our preliminary results (not included in the paper) also suggest that *correlation-only models can use much less training data and are less prone to overfitting to the similarity loss* compared to intensity feature-based models. In our experiments, intensity feature-based models degrade considerably when no regularization is used, whereas correlation-only models remain robust.

Acknowledgments. This study was funded by NIH (R01CA188300) and DOD (W81XWH2210044).

Disclosure of Interests. The authors have no competing interests to declare that are relevant to the content of this article.

References

1. Dufumier, B., Grigis, A., Victor, J., Ambroise, C., Frouin, V., Duchesnay, E.: OpenBHB: a Large-Scale Multi-Site Brain MRI Data-set for Age Prediction and Debiasing. *NeuroImage*. 263, 119637 (2022). <https://doi.org/10.1016/j.neuroimage.2022.119637>.
2. Taha, A., Gilmore, G., Abbass, M., Kai, J., Kuehn, T., Demarco, J., Gupta, G., Zajner, C., Cao, D., Chevalier, R., Ahmed, A., Hadi, A., Karat, B.G., Stanley, O.W., Park, P.J., Ferko, K.M., Hemachandra, D., Vassallo, R., Jach, M., Thurairajah, A., Wong, S., Tenorio, M.C., Ogunsanya, F., Khan, A.R., Lau, J.C.: Magnetic resonance imaging datasets with anatomical fiducials for quality control and registration. *Sci. Data.* 10, 449 (2023). <https://doi.org/10.1038/s41597-023-02330-9>.
3. Chen, J., Wei, S., Honkamaa, J., Marttinen, P., Zhang, H., Liu, M., Zhou, Y., Tan, Z., Wang, Z., Wang, Y., Zhou, H., Hu, S., Zhang, Y., Tao, Q., Förner, L., Wendler, T., Jian, B., Wiestler, B., Hable, T., Kim, J., Ruan, D., Madesta, F., Sentker, T., Heyer, W., Zuo, L., Dai, Y., Wu, J., Prince, J.L., Bai, H., Du, Y., Liu, Y., Hering, A., Dorent, R., Hansen, L., Heinrich, M.P., Carass, A.: Beyond the LUMIR challenge: The pathway to foundational registration models, <http://arxiv.org/abs/2505.24160>, (2025). <https://doi.org/10.48550/arXiv.2505.24160>.
4. Honkamaa, J., Marttinen, P.: SITReg: Multi-resolution architecture for symmetric, inverse consistent, and topology preserving image registration. *Mach. Learn. Biomed. Imaging.* 2, 2148–2194 (2024). <https://doi.org/10.59275/j.melba.2024-276b>.
5. Liu, Y., Chen, J., Zuo, L., Carass, A., Prince, J.L.: Vector field attention for deformable image registration. *J. Med. Imaging.* 11, 064001 (2024). <https://doi.org/10.1117/1.JMI.11.6.064001>.
6. Heinrich, M.P.: Closing the Gap Between Deep and Conventional Image Registration Using Probabilistic Dense Displacement Networks. In: Shen, D., Liu, T., Peters, T.M., Staib, L.H., Essert, C., Zhou, S., Yap, P.-T., and Khan, A. (eds.) *Medical Image Computing and Computer Assisted Intervention – MICCAI 2019*. pp. 50–58. Springer International Publishing, Cham (2019). https://doi.org/10.1007/978-3-030-32226-7_6.
7. Jian, B., Pan, J., Ghahremani, M., Rueckert, D., Wachinger, C., Wiestler, B.: Mamba? Catch The Hype Or Rethink What Really Helps for Image Registration, <http://arxiv.org/abs/2407.19274>, (2024). <https://doi.org/10.48550/arXiv.2407.19274>.
8. Liu, H., Ruan, D., Sheng, K.: Unsupervised Deformable Image Registration Revisited: Enhancing Performance with Registration-Specific Designs. Presented at the Medical Imaging with Deep Learning - Short Papers April 12 (2025).
9. Jian, B., Pan, J., Jena, R., Ghahremani, M., Li, H.B., Rueckert, D., Wachinger, C., Wiestler, B.: Disentangling Progress in Medical Image Registration: Beyond Trend-Driven Architectures towards Domain-Specific Strategies, <http://arxiv.org/abs/2512.01913>, (2025). <https://doi.org/10.48550/arXiv.2512.01913>.
10. Heinrich, M.P., Jenkinson, M., Bhushan, M., Matin, T., Gleeson, F.V., Brady, S.M., Schnabel, J.A.: MIND: Modality independent neighbourhood descriptor for multi-modal deformable registration. *Med. Image Anal.* 16, 1423–1435 (2012). <https://doi.org/10.1016/j.media.2012.05.008>.
11. Balakrishnan, G., Zhao, A., Sabuncu, M.R., Guttag, J., Dalca, A.V.: VoxelMorph: A Learning Framework for Deformable Medical Image Registration. *IEEE Trans. Med. Imaging.* 38, 1788–1800 (2019). <https://doi.org/10.1109/TMI.2019.2897538>.

12. Chen, J., Frey, E.C., He, Y., Segars, W.P., Li, Y., Du, Y.: TransMorph: Transformer for unsupervised medical image registration. *Med. Image Anal.* 82, 102615 (2022). <https://doi.org/10.1016/j.media.2022.102615>.
13. Liu, Y., Chen, J., Wei, S., Carass, A., Prince, J.: On Finite Difference Jacobian Computation in Deformable Image Registration. *Int. J. Comput. Vis.* 132, 3678–3688 (2024). <https://doi.org/10.1007/s11263-024-02047-1>.
14. Su, Z., Yao, K., Yang, X., Huang, K., Wang, Q., Sun, J.: Rethinking data augmentation for single-source domain generalization in medical image segmentation. In: Proceedings of the Thirty-Seventh AAAI Conference on Artificial Intelligence and Thirty-Fifth Conference on Innovative Applications of Artificial Intelligence and Thirteenth Symposium on Educational Advances in Artificial Intelligence. pp. 2366–2374. AAAI Press (2023). <https://doi.org/10.1609/aaai.v37i2.25332>.
15. Iglesias, J.E., Billot, B., Balbastre, Y., Tabari, A., Conklin, J., Gilberto González, R., Alexander, D.C., Golland, P., Edlow, B.L., Fischl, B.: Joint super-resolution and synthesis of 1 mm isotropic MP-RAGE volumes from clinical MRI exams with scans of different orientation, resolution and contrast. *NeuroImage*. 237, 118206 (2021). <https://doi.org/10.1016/j.neuroimage.2021.118206>.
16. Honkamaa, J., Marttinen, P.: Strategies for Robust Deep Learning Based Deformable Registration, <http://arxiv.org/abs/2510.23079>, (2025). <https://doi.org/10.48550/arXiv.2510.23079>.
17. Dosovitskiy, A., Fischer, P., Ilg, E., Hausser, P., Hazirbas, C., Golkov, V., Smagt, P.V.D., Cremers, D., Brox, T.: FlowNet: Learning Optical Flow with Convolutional Networks. In: 2015 IEEE International Conference on Computer Vision (ICCV). pp. 2758–2766. IEEE, Santiago (2015). <https://doi.org/10.1109/ICCV.2015.316>.